

# Optimization of universal quantum gates with higher-dimensional spaces

Wen-Qiang Liu<sup>1,2</sup>, Hai-Rui Wei<sup>1</sup>, and Leong-Chuan Kwek<sup>3,4,5</sup>

<sup>1</sup>School of Mathematics and Physics, University of Science and Technology Beijing, Beijing 100083, China

<sup>2</sup>Center for Quantum Technology Research and Key Laboratory of Advanced Optoelectronic Quantum Architecture and Measurements (MOE), School of Physics, Beijing Institute of Technology, Beijing 100081, China

<sup>3</sup>Centre for Quantum Technologies, National University of Singapore, Singapore 117543, Singapore

<sup>4</sup>MajuLab, CNRS-UNS-NUS-NTU International Joint Research Unit, Singapore UMI 3654, Singapore

<sup>5</sup>National Institute of Education and Institute of Advanced Studies, Nanyang Technological University, Singapore 637616, Singapore

**Minimizing the number of necessary two-qubit gates is an important task in quantum information processing. By introducing non-computational quantum states, we construct effective circuits for the controlled-NOT (CNOT) gate and the  $n$ -qubit Toffoli gate with  $(2n - 3)$  qubit-qudit gates and  $(2n - 4)$  single-qudit gates. The cost of a three-qubit Toffoli gate is reduced from the minimum limit of five two-qubit gates to three nearest-neighbor qubit-qudit gates. By operating with the spatial-mode degree of freedom, polarization CNOT and Toffoli gates are designed with linear optics. Our optical schemes can be achieved with a higher success probability and no extra auxiliary photons are needed in the scheme.**

## 1 Introduction

Multi-qubit quantum gates have complex structures and play an important role in quantum computing [1], quantum algorithms [2–5], cryptography [6], etc. [7]. The most popular paradigm for implementing a quantum gate is the quantum circuit model [1]. However, when the cost (also called complexity) of the quantum circuit (measured by the number of two-qubit gates involved in a quantum circuit) is high, it is difficult to perform the experiments because of the low computing fidelity and limited coherence time. Moreover, the cost of a universal quantum circuit increases exponentially as the number of qubits

Hai-Rui Wei: hrwei@ustb.edu.cn

increases. The theoretical lower bound for simulating an  $n$ -qubit universal quantum circuit is  $(4^n - 3n - 1)/4$  controlled-NOT (CNOT) gates in qubit system [8]. Hence, it is crucial to find an effective method for building a universal quantum circuit in the simplest possible way.

Several matrix decomposition techniques have been introduced to optimize a large-scale quantum circuit [9–15]. Two-qubit universal quantum circuits have also been constructed with the lowest cost (resources) in qubit systems [8, 16–18]. However, there is still a gap between the current best result [12] and the theoretical lower bound [8] for a multi-qubit universal quantum circuit. Fortunately, Ralph *et al.* [19] found that the quantum circuit may be optimized further by using higher-dimensional Hilbert spaces, and this proposal was later experimentally demonstrated in optical [20] and superconducting systems [21]. Following this, Liu *et al.* [22, 23] reduced the cost of the  $n$ -qubit universal circuit to  $(5/16) \times 4^n - (5/4) \times 2^n + 2n$  CNOT gates when  $n$  was even and  $(5/16) \times 4^n - 2^n + 2(n - 1)$  CNOTs when  $n$  was odd. Liu *et al.* simplified a Fredkin gate from eight CNOTs to five CNOTs [24] or three qubit-qudit gates [25]. In addition, higher-dimensional systems have also been used in the optimization of quantum communication [26–32] and quantum metrology [33].

The Toffoli (controlled-NOT-NOT) gate, a three-qubit conditional operation, is one of the most popular universal multi-qubit quantum gates [34]. It is also an essential component in complex quantum algorithms [2–5], quantum error correction [35, 36], and quantum fault toler-

ance [37, 38]. In 1995, Barenco *et al.* [1] proposed a concrete construction of a three-qubit Toffoli gate with five two-qubit entangled gates. When two-qubit gates are restricted to CNOT gates, the optimal cost of a Toffoli gate increases to six [39]. In 2013, Yu *et al.* [40, 41] confirmed that the minimum resource for simulating a three-qubit Toffoli gate is five two-qubit gates. In 2020, Kiktenko *et al.* [42] constructed a generalized  $m$ -qubit Toffoli gate with  $(2m-3)$  CNOTs based on qudits. Independent of the standard decomposition-based approach, Toffoli gates have been implemented experimentally in superconducting circuits [21, 36], linear optics [20, 43–46], trapped ions [47], atoms [48, 49], and quantum dots [50].

In this paper, we propose a simplified CNOT and multi-qubit Toffoli gates by using higher-dimensional spaces. Specifically,  $(2n-3)$  qubit-qudit and  $(2n-4)$  single-qudit gates are required to implement an  $n$ -qubit Toffoli gate. The cost of the three-qubit Toffoli gate is reduced from the lower bound of five two-qubit gates to one CNOT and two partial-swap (P-SWAP) gates. In addition, using the spatial-mode degree of freedom (DOF) of the single photon, we design a feasible optical architecture for implementing CNOT and Toffoli gates with linear optics. Our proposals have several other advantages: (i) Our optical implementation of the CNOT gate does not require an extra entangled photon pair or a single photon, and the success probability of the gate is enhanced. (ii) The cost of the three-qubit Toffoli gate is reduced from the unconstructed lower bound of five two-qubit gates [40, 41] three qubit-qudit gates. (iii) Linear optical Toffoli gates can be constructed with a higher success probability than other existing optical schemes [19, 20, 51].

## 2 Construction of CNOT and Toffoli gates with higher-dimensional spaces

We focus on the simplification of controlled quantum gates with minimal resource overheads, and the main idea of our proposal is to extend temporarily the higher-dimensional subspaces on one of the controlled qubit carriers and then perform corresponding logical operations.

### 2.1 Synthesis of a CNOT gate using qutrits

A CNOT gate with two P-SWAP gates using qutrits is shown in Fig. 1. The gate qubits are encoded on two computational states,  $|0\rangle$  and  $|1\rangle$ . The single-qutrit  $X_A$  gate provides a three-dimensional subspace on the control qubit. In the following, we describe the construction process of our protocol in detail.

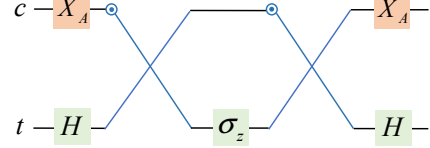


Figure 1: Synthesis of a CNOT gate. The single-qutrit  $X_A$  gate implements the transformation  $|1\rangle \leftrightarrow |2\rangle$ . The controlled node  $\odot$  is turned on for the input  $|0\rangle$  or  $|1\rangle$ . That is, a swap operation is applied to  $c$  and  $t$ , if and only if, the control qubit  $c$  is in the state  $|0\rangle$  or  $|1\rangle$ .  $H$  is a single-qubit Hadamard gate to achieve operations  $|0\rangle \leftrightarrow \frac{1}{\sqrt{2}}(|0\rangle + |1\rangle)$  and  $|1\rangle \leftrightarrow \frac{1}{\sqrt{2}}(|0\rangle - |1\rangle)$ .  $\sigma_z$  completes  $\sigma_z|0\rangle = |0\rangle$  and  $\sigma_z|1\rangle = -|1\rangle$ .

Suppose that the state of the system is initially

$$|\phi_0\rangle = \alpha_1|0_c\rangle|0_t\rangle + \alpha_2|0_c\rangle|1_t\rangle + \alpha_3|1_c\rangle|0_t\rangle + \alpha_4|1_c\rangle|1_t\rangle. \quad (1)$$

where  $\alpha_i$  ( $i = 1, 2, 3, 4$ ) are complex coefficients that satisfy the normalization condition  $\sum_{i=1}^4 |\alpha_i|^2 = 1$ . Subscripts  $c$  and  $t$  denote the control and target qubits, respectively.

First, qubit  $c$  undergoes a single-qutrit gate  $X_A$ , which introduces an ancillary state  $|2\rangle$  on  $c$  and completes the transformations  $|1_c\rangle \xrightarrow{X_A} |2_c\rangle$  and  $|0_c\rangle \xrightarrow{X_A} |0_c\rangle$ . After the  $X_A$  gate and a Hadamard ( $H$ ) gate are applied to  $c$  and  $t$ , the initial state  $|\phi_0\rangle$  is changed to

$$|\phi_1\rangle = \frac{1}{\sqrt{2}}[\alpha_1|0_c\rangle(|0_t\rangle + |1_t\rangle) + \alpha_2|0_c\rangle(|0_t\rangle - |1_t\rangle) + \alpha_3|2_c\rangle(|0_t\rangle + |1_t\rangle) + \alpha_4|2_c\rangle(|0_t\rangle - |1_t\rangle)]. \quad (2)$$

Second, a P-SWAP gate is applied to  $c$  and  $t$ , and it transforms  $|\phi_1\rangle$  into

$$|\phi_2\rangle = \frac{1}{\sqrt{2}}[\alpha_1(|0_c\rangle + |1_c\rangle)|0_t\rangle + \alpha_2(|0_c\rangle - |1_c\rangle)|0_t\rangle + \alpha_3|2_c\rangle(|0_t\rangle + |1_t\rangle) + \alpha_4|2_c\rangle(|0_t\rangle - |1_t\rangle)]. \quad (3)$$

Here, the P-SWAP gate performs a swap operation only between two computational states  $|0\rangle$  and  $|1\rangle$ , that is,

$$\begin{aligned} |00\rangle &\xrightarrow{\text{P-SWAP}} |00\rangle, & |01\rangle &\xrightarrow{\text{P-SWAP}} |10\rangle, \\ |10\rangle &\xrightarrow{\text{P-SWAP}} |01\rangle, & |11\rangle &\xrightarrow{\text{P-SWAP}} |11\rangle, \\ |20\rangle &\xrightarrow{\text{P-SWAP}} |20\rangle, & |21\rangle &\xrightarrow{\text{P-SWAP}} |21\rangle. \end{aligned} \quad (4)$$

Third, a  $\sigma_z$  operation acts on  $t$  to change  $|\phi_2\rangle$  to

$$\begin{aligned} |\phi_3\rangle = \frac{1}{\sqrt{2}} &[\alpha_1(|0_c\rangle + |1_c\rangle)|0_t\rangle \\ &+ \alpha_2(|0_c\rangle - |1_c\rangle)|0_t\rangle \\ &+ \alpha_3|2_c\rangle(|0_t\rangle - |1_t\rangle) \\ &+ \alpha_4|2_c\rangle(|0_t\rangle + |1_t\rangle)]. \end{aligned} \quad (5)$$

Finally, after the P-SWAP gate, the  $X_A$  gate and  $H$  operation are applied to  $c$  and  $t$  again,  $|\phi_3\rangle$  is changed to

$$\begin{aligned} |\phi_4\rangle = &\alpha_1|0_c\rangle|0_t\rangle + \alpha_2|0_c\rangle|1_t\rangle \\ &+ \alpha_3|1_c\rangle|1_t\rangle + \alpha_4|1_c\rangle|0_t\rangle. \end{aligned} \quad (6)$$

Note that Eq. (6) is a CNOT gate, and such a construction can be achieved in linear optics with a high success probability and without additional photons (see Sec. 3).

## 2.2 Construction of Toffoli gates with higher-dimensional spaces

### 2.2.1 Synthesis of a three-qubit Toffoli gate using qutrits

Based on the designed CNOT and P-SWAP gates, the process for implementing a three-qubit Toffoli gate with four-dimensional space is presented in Fig. 2.

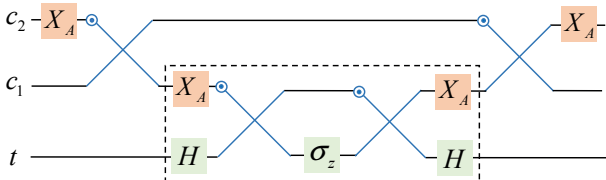


Figure 2: Simplified synthesis of a three-qubit Toffoli gate with two P-SWAP and one CNOT gates. As shown in Fig. 1, the operations in the dotted rectangle are a CNOT gate.

Considering an arbitrary normalization three-qubit initial state

$$\begin{aligned} |\psi_0\rangle = &\alpha_1|0_{c_1}\rangle|0_{c_2}\rangle|0_t\rangle + \alpha_2|0_{c_1}\rangle|0_{c_2}\rangle|1_t\rangle, \\ &+ \alpha_3|0_{c_1}\rangle|1_{c_2}\rangle|0_t\rangle + \alpha_4|0_{c_1}\rangle|1_{c_2}\rangle|1_t\rangle \\ &+ \alpha_5|1_{c_1}\rangle|0_{c_2}\rangle|0_t\rangle + \alpha_6|1_{c_1}\rangle|0_{c_2}\rangle|1_t\rangle \\ &+ \alpha_7|1_{c_1}\rangle|1_{c_2}\rangle|0_t\rangle + \alpha_8|1_{c_1}\rangle|1_{c_2}\rangle|1_t\rangle. \end{aligned} \quad (7)$$

First, the  $X_A$  gate acts on  $c_2$  to achieve  $|1_{c_2}\rangle \xrightarrow{X_A} |2_{c_2}\rangle$  and  $|0_{c_2}\rangle \xrightarrow{X_A} |0_{c_2}\rangle$ . After the first P-SWAP gate is executed on  $c_1$  and  $c_2$ ,  $|\psi_0\rangle$  becomes

$$\begin{aligned} |\psi_1\rangle = &\alpha_1|0_{c_1}\rangle|0_{c_2}\rangle|0_t\rangle + \alpha_2|0_{c_1}\rangle|0_{c_2}\rangle|1_t\rangle, \\ &+ \alpha_3|0_{c_1}\rangle|2_{c_2}\rangle|0_t\rangle + \alpha_4|0_{c_1}\rangle|2_{c_2}\rangle|1_t\rangle \\ &+ \alpha_5|0_{c_1}\rangle|1_{c_2}\rangle|0_t\rangle + \alpha_6|0_{c_1}\rangle|1_{c_2}\rangle|1_t\rangle \\ &+ \alpha_7|1_{c_1}\rangle|2_{c_2}\rangle|0_t\rangle + \alpha_8|1_{c_1}\rangle|2_{c_2}\rangle|1_t\rangle. \end{aligned} \quad (8)$$

Second, a CNOT gate is applied to  $c_1$  and  $t$  (which can be achieved by the circuit in the dotted rectangle), resulting in

$$\begin{aligned} |\psi_2\rangle = &\alpha_1|0_{c_1}\rangle|0_{c_2}\rangle|0_t\rangle + \alpha_2|0_{c_1}\rangle|0_{c_2}\rangle|1_t\rangle, \\ &+ \alpha_3|0_{c_1}\rangle|2_{c_2}\rangle|0_t\rangle + \alpha_4|0_{c_1}\rangle|2_{c_2}\rangle|1_t\rangle \\ &+ \alpha_5|0_{c_1}\rangle|1_{c_2}\rangle|0_t\rangle + \alpha_6|0_{c_1}\rangle|1_{c_2}\rangle|1_t\rangle \\ &+ \alpha_7|1_{c_1}\rangle|2_{c_2}\rangle|1_t\rangle + \alpha_8|1_{c_1}\rangle|2_{c_2}\rangle|0_t\rangle. \end{aligned} \quad (9)$$

Finally, the P-SWAP and  $X_A$  gates are applied again. The two operations induce  $|\psi_2\rangle$  as the final state

$$\begin{aligned} |\psi_3\rangle = &\alpha_1|0_{c_1}\rangle|0_{c_2}\rangle|0_t\rangle + \alpha_2|0_{c_1}\rangle|0_{c_2}\rangle|1_t\rangle, \\ &+ \alpha_3|0_{c_1}\rangle|1_{c_2}\rangle|0_t\rangle + \alpha_4|0_{c_1}\rangle|1_{c_2}\rangle|1_t\rangle \\ &+ \alpha_5|1_{c_1}\rangle|0_{c_2}\rangle|0_t\rangle + \alpha_6|1_{c_1}\rangle|0_{c_2}\rangle|1_t\rangle \\ &+ \alpha_7|1_{c_1}\rangle|1_{c_2}\rangle|1_t\rangle + \alpha_8|1_{c_1}\rangle|1_{c_2}\rangle|0_t\rangle. \end{aligned} \quad (10)$$

From Eqs. (7-10), one can see that a three-qubit Toffoli gate can be simulated using three nearest-neighbor qubit-qutrit gates and two single-qutrit gates. The cost of this construction outperforms the previous synthesis ones that require six CNOT gates [39] or five two-qubit gates [1].

### 2.2.2 Synthesis of $n$ -control-qubit Toffoli gate using qutrits

Using a higher-dimensional space, the method can be applied to any multi-qubit Toffoli gate. As shown in Fig. 3, an  $n$ -control-qubit Toffoli gate is constructed with  $(2n - 1)$  qubit-qutrit and

$(2n - 2)$  single-qudit gates, which flips the target qubit states  $|0\rangle$  and  $|1\rangle$  if and only if the  $n$  control-qubits are all  $|1\rangle$ . Here, single-qudit gates  $X_a, X_b, \dots, X_n$  create multi-level qudits on  $c_n$  and complete transformations  $|0_{c_n}\rangle \leftrightarrow |2_{c_n}\rangle$ ,  $|1_{c_n}\rangle \leftrightarrow |3_{c_n}\rangle$ ,  $|0_{c_n}\rangle \leftrightarrow |4_{c_n}\rangle$ ,  $\dots$ ,  $|0_{c_n}\rangle \leftrightarrow |n_{c_n}\rangle$  when  $n$  is even or  $|0_{c_n}\rangle \leftrightarrow |2_{c_n}\rangle$ ,  $|1_{c_n}\rangle \leftrightarrow |3_{c_n}\rangle$ ,  $|0_{c_n}\rangle \leftrightarrow |4_{c_n}\rangle$ ,  $\dots$ ,  $|1_{c_n}\rangle \leftrightarrow |n_{c_n}\rangle$  when  $n$  is odd. These single-qudit gates can temporarily expand the two-dimensional space of  $c_n$  to an  $(n+1)$ -dimensional subspace. All CNOT and P-SWAP gates act on computational states  $|0\rangle$  and  $|1\rangle$ . The synthesis requires  $O(n)$  qubit-qudit gates, which is considerably less than the previous result, which required  $O(n^2)$  CNOT gates [1]. The low-cost advantage is more evident in our scheme as the number of qubits increases.

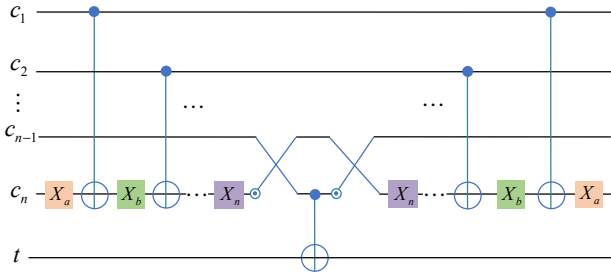


Figure 3: Synthesis of an  $n$ -control-qubit Toffoli gate in a higher-dimensional space. Single-qudit gates  $X_a, X_b, \dots, X_n$  complete operations  $|0_{c_n}\rangle \leftrightarrow |2_{c_n}\rangle$ ,  $|1_{c_n}\rangle \leftrightarrow |3_{c_n}\rangle$ ,  $\dots$ ,  $|0_{c_n}\rangle \leftrightarrow |n_{c_n}\rangle$  when  $n$  is even or  $|0_{c_n}\rangle \leftrightarrow |2_{c_n}\rangle$ ,  $|1_{c_n}\rangle \leftrightarrow |3_{c_n}\rangle$ ,  $\dots$ ,  $|1_{c_n}\rangle \leftrightarrow |n_{c_n}\rangle$  when  $n$  is odd, respectively.

### 3 Implementation of linear optical CNOT and Toffoli gates

In the previous section, we proposed the simulation of CNOT and Toffoli gates based on P-SWAP gates and auxiliary higher-dimensional spaces. In an optical system, two computational states can be encoded on the polarization DOF of a single photon in the spatial-mode  $i$ , that is,  $|0\rangle \equiv |H\rangle_i$  and  $|1\rangle \equiv |V\rangle_i$ . Here,  $H$  and  $V$  represent the horizontal and vertical polarized components, respectively. The higher-dimensional state can be encoded on the  $V$ -polarized component in a new spatial-mode  $i'$ , that is,  $|2\rangle \equiv |V\rangle_{i'}$ . The qubit operation  $X_A$  can be achieved by employing a polarizing beam splitter (PBS), which reflects the  $V$ -polarized component and transmits the  $H$ -polarized component, respectively. Before

describing the implementation of the CNOT gate, we first detail the step-by-step construction of the P-SWAP gate with linear optical elements.

As shown in Fig. 4, the injected photon 1 is divided into  $H$ -polarized component and  $V$ -polarized component by a PBS. The  $H$ -polarized component passes into the spatial-mode  $1_{in}$ , which is encoded on  $|H\rangle_{1_{in}} \equiv |0\rangle$  (and  $V$ -polarized component in the spatial-mode  $1_{in}$  is encoded on  $|V\rangle_{1_{in}} \equiv |1\rangle$ ), while the  $V$ -polarized component is reflected into another spatial-mode  $1'_{in}$ , which is encoded on  $|V\rangle_{1'_{in}} \equiv |2\rangle$ . The photon 2 from the spatial-mode  $2_{in}$  is encoded on  $|H\rangle_{2_{in}} \equiv |0\rangle$  and  $|V\rangle_{2_{in}} \equiv |1\rangle$ . A general injected photon state can be considered as

$$|\varphi_0\rangle = \alpha_1 |H\rangle_{1_{in}} |H\rangle_{2_{in}} + \alpha_2 |H\rangle_{1_{in}} |V\rangle_{2_{in}} + \alpha_3 |V\rangle_{1_{in}} |H\rangle_{2_{in}} + \alpha_4 |V\rangle_{1_{in}} |V\rangle_{2_{in}} + \alpha_5 |V\rangle_{1'_{in}} |H\rangle_{2_{in}} + \alpha_6 |V\rangle_{1'_{in}} |V\rangle_{2_{in}}. \quad (11)$$

First, PBS<sub>1</sub> and PBS<sub>2</sub> transmit the  $H$ -photons into modes 1 and 3 to interact with half-wave plates HWP<sup>45°</sup> and HWP<sup>22.5°</sup> and reflect the  $V$ -photons into modes 2 and 4 to interact with HWP<sup>45°</sup> and HWP<sup>67.5°</sup>. Here, HWP<sup>45°</sup> is a half-wave plate set to 45 degrees and achieves the qubit-flip operation  $|H\rangle \leftrightarrow |V\rangle$ . HWP<sup>22.5°</sup> completes the transformations

$$\begin{aligned} |H\rangle &\xrightarrow{\text{HWP}^{22.5^\circ}} \frac{1}{\sqrt{2}}(|H\rangle + |V\rangle), \\ |V\rangle &\xrightarrow{\text{HWP}^{22.5^\circ}} \frac{1}{\sqrt{2}}(|H\rangle - |V\rangle). \end{aligned} \quad (12)$$

HWP<sup>67.5°</sup> results in

$$\begin{aligned} |H\rangle &\xrightarrow{\text{HWP}^{67.5^\circ}} \frac{1}{\sqrt{2}}(-|H\rangle + |V\rangle), \\ |V\rangle &\xrightarrow{\text{HWP}^{67.5^\circ}} \frac{1}{\sqrt{2}}(|H\rangle + |V\rangle). \end{aligned} \quad (13)$$

The above operations, PBS<sub>1</sub>  $\rightarrow$  HWP<sup>45°</sup> (HWP<sup>45°</sup>) and PBS<sub>2</sub>  $\rightarrow$  HWP<sup>22.5°</sup> (HWP<sup>67.5°</sup>) cause  $|\varphi_0\rangle$  to become

$$\begin{aligned} |\varphi_1\rangle = &\frac{1}{\sqrt{2}}[\alpha_1 |V\rangle_1 (|H\rangle_3 + |V\rangle_3) \\ &+ \alpha_2 |V\rangle_1 (|H\rangle_4 + |V\rangle_4) \\ &+ \alpha_3 |H\rangle_2 (|H\rangle_3 + |V\rangle_3) \\ &+ \alpha_4 |H\rangle_2 (|H\rangle_4 + |V\rangle_4) \\ &+ \alpha_5 |V\rangle_{1'_{in}} (|H\rangle_3 + |V\rangle_3) \\ &+ \alpha_6 |V\rangle_{1'_{in}} (|H\rangle_4 + |V\rangle_4)]. \end{aligned} \quad (14)$$

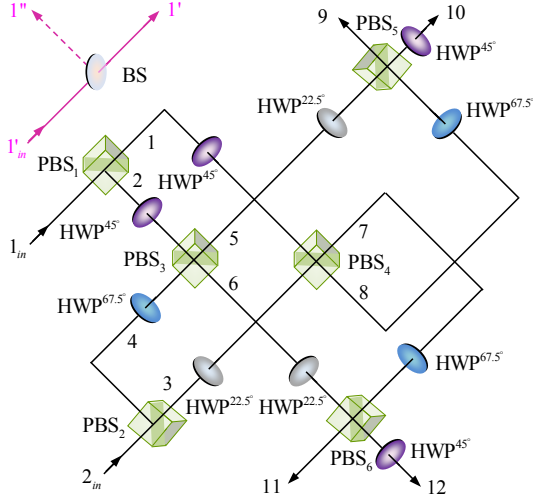


Figure 4: Implementation of a linear optical P-SWAP gate. The half-wave plate  $\text{HWP}^{45^\circ}$  realizes the qubit-flip  $|H\rangle \leftrightarrow |V\rangle$ .  $\text{HWP}^{22.5^\circ}$  completes the operations  $|H\rangle \leftrightarrow \frac{1}{\sqrt{2}}(|H\rangle + |V\rangle)$  and  $|V\rangle \leftrightarrow \frac{1}{\sqrt{2}}(|H\rangle - |V\rangle)$ , and  $\text{HWP}^{67.5^\circ}$  completes  $|H\rangle \leftrightarrow \frac{1}{\sqrt{2}}(-|H\rangle + |V\rangle)$  and  $|V\rangle \leftrightarrow \frac{1}{\sqrt{2}}(|H\rangle + |V\rangle)$ . BS is a balanced beam splitter to realize  $|V\rangle_{1'_in} \leftrightarrow \frac{1}{\sqrt{2}}(|V\rangle_{1'} + |V\rangle_{1''})$ .

Photons in mode  $1'_in$  are then split into modes  $1'$  and  $1''$  by a balanced polarization beam splitter (BS), i.e.,  $|V\rangle_{1'_in} \xrightarrow{\text{BS}} (|V\rangle_{1'} + |V\rangle_{1''})/\sqrt{2}$ . Photons emitted from modes 2 and 4 (1 and 3) are split into modes 5 and 6 (7 and 8) by  $\text{PBS}_3$  ( $\text{PBS}_4$ ) and followed by  $\text{HWP}^{22.5^\circ}$  ( $\text{HWP}^{67.5^\circ}$ ). These elements change  $|\varphi_1\rangle$  as

$$\begin{aligned}
|\varphi_2\rangle = & \frac{1}{2\sqrt{2}}[\alpha_1(|H\rangle_7 + |V\rangle_7)(-|H\rangle_7 + |V\rangle_7 \\
& + |H\rangle_8 + |V\rangle_8) + \alpha_2(|H\rangle_7 + |V\rangle_7) \\
& \times (|H\rangle_5 + |V\rangle_5 + |H\rangle_6 - |V\rangle_6) \\
& + \alpha_3(|H\rangle_6 + |V\rangle_6)(-|H\rangle_7 + |V\rangle_7 \\
& + |H\rangle_8 + |V\rangle_8) + \alpha_4(|H\rangle_6 + |V\rangle_6) \\
& \times (|H\rangle_5 + |V\rangle_5 + |H\rangle_6 - |V\rangle_6) \\
& + \alpha_5(|V\rangle_{1'} + |V\rangle_{1''})(-|H\rangle_7 + |V\rangle_7 \\
& + |H\rangle_8 + |V\rangle_8) + \alpha_6(|V\rangle_{1'} + |V\rangle_{1''}) \\
& \times (|H\rangle_5 + |V\rangle_5 + |H\rangle_6 - |V\rangle_6)].
\end{aligned} \tag{15}$$

Finally,  $\text{PBS}_5$  ( $\text{PBS}_6$ ) induces photons into modes 9 and 10 (11 and 12). Photons in modes 10 and 12 will undergo  $\text{HWP}^{45^\circ}$ . Thus, the state

of the system evolves as

$$\begin{aligned}
|\varphi_3\rangle = & \frac{1}{2\sqrt{2}}[\alpha_1(|H\rangle_{11} + |H\rangle_{12})(-|H\rangle_{11} + |H\rangle_{12} \\
& + |H\rangle_9 + |H\rangle_{10}) + \alpha_2(|H\rangle_{11} + |H\rangle_{12}) \\
& \times (|V\rangle_{10} + |V\rangle_9 + |V\rangle_{12} - |V\rangle_{11}) \\
& + \alpha_3(|V\rangle_{12} + |V\rangle_{11})(-|H\rangle_{11} + |H\rangle_{12} \\
& + |H\rangle_9 + |H\rangle_{10}) + \alpha_4(|V\rangle_{12} + |V\rangle_{11}) \\
& \times (|V\rangle_{10} + |V\rangle_9 + |V\rangle_{12} - |V\rangle_{11}) \\
& + \alpha_5(|V\rangle_{1'} + |V\rangle_{1''})(-|H\rangle_{11} + |H\rangle_{12} \\
& + |H\rangle_9 + |H\rangle_{10}) + \alpha_6(|V\rangle_{1'} + |V\rangle_{1''}) \\
& \times (|V\rangle_{10} + |V\rangle_9 + |V\rangle_{12} - |V\rangle_{11})].
\end{aligned} \tag{16}$$

As shown in Table 1, there are four desired coincidence outcomes in the construction of the post-selection P-SWAP gate. (i) When the detected output modes are 9,  $1'$ , and 12, the state  $|\varphi_3\rangle$  will collapse into

$$\begin{aligned}
|\varphi_4^1\rangle = & \frac{1}{2\sqrt{2}}(\alpha_1|H\rangle_9|H\rangle_{12} + \alpha_2|V\rangle_9|H\rangle_{12} \\
& + \alpha_3|H\rangle_9|V\rangle_{12} + \alpha_4|V\rangle_9|V\rangle_{12} \\
& + \alpha_5|V\rangle_{1'}|H\rangle_{12} + \alpha_6|V\rangle_{1'}|V\rangle_{12}).
\end{aligned} \tag{17}$$

(ii) When the detected output modes are 10,  $1'$ , and 12, the state  $|\varphi_3\rangle$  will collapse into

$$\begin{aligned}
|\varphi_4^2\rangle = & \frac{1}{2\sqrt{2}}(\alpha_1|H\rangle_{10}|H\rangle_{12} + \alpha_2|V\rangle_{10}|H\rangle_{12} \\
& + \alpha_3|H\rangle_{10}|V\rangle_{12} + \alpha_4|V\rangle_{10}|V\rangle_{12} \\
& + \alpha_5|V\rangle_{1'}|H\rangle_{12} + \alpha_6|V\rangle_{1'}|V\rangle_{12}).
\end{aligned} \tag{18}$$

(iii) When the detected output modes are 9,  $1'$ , and 11, the state  $|\varphi_3\rangle$  will collapse into

$$\begin{aligned}
|\varphi_4^3\rangle = & \frac{1}{2\sqrt{2}}(\alpha_1|H\rangle_9|H\rangle_{11} + \alpha_2|V\rangle_9|H\rangle_{11} \\
& + \alpha_3|H\rangle_9|V\rangle_{11} + \alpha_4|V\rangle_9|V\rangle_{11} \\
& - \alpha_5|V\rangle_{1'}|H\rangle_{11} - \alpha_6|V\rangle_{1'}|V\rangle_{11}).
\end{aligned} \tag{19}$$

(iv) When the detected output modes are 10,  $1'$ , and 11, the state  $|\varphi_3\rangle$  will collapse into

$$\begin{aligned}
|\varphi_4^4\rangle = & \frac{1}{2\sqrt{2}}(\alpha_1|H\rangle_{10}|H\rangle_{11} + \alpha_2|V\rangle_{10}|H\rangle_{11} \\
& + \alpha_3|H\rangle_{10}|V\rangle_{11} + \alpha_4|V\rangle_{10}|V\rangle_{11} \\
& - \alpha_5|V\rangle_{1'}|H\rangle_{11} - \alpha_6|V\rangle_{1'}|V\rangle_{11}).
\end{aligned} \tag{20}$$

According to Eq. (17) to Eq. (20), one can see that when the outgoing components emitting from modes 9,  $1'$ , and 12 (or from 10,  $1'$ ,

Table 1: Coincident expectation outgoing values for six logic basis inputs.  $\langle n_{H_i/V_i} n_{H_j/V_j} \rangle$  is the number of  $H/V$ -photons detected in modes  $i$  and  $j$ .

Input	$\langle n_{H_9} n_{H_{12}} \rangle$	$\langle n_{V_9} n_{H_{12}} \rangle$	$\langle n_{H_9} n_{V_{12}} \rangle$	$\langle n_{V_9} n_{V_{12}} \rangle$	$\langle n_{V_{1'}} n_{H_{12}} \rangle$	$\langle n_{V_{1'}} n_{V_{12}} \rangle$
	$\langle n_{H_{10}} n_{H_{12}} \rangle$	$\langle n_{V_{10}} n_{H_{12}} \rangle$	$\langle n_{H_{10}} n_{V_{12}} \rangle$	$\langle n_{V_{10}} n_{V_{12}} \rangle$	$\langle n_{V_{1'}} n_{H_{12}} \rangle$	$\langle n_{V_{1'}} n_{V_{12}} \rangle$
	$\langle n_{H_9} n_{H_{11}} \rangle$	$\langle n_{V_9} n_{H_{11}} \rangle$	$\langle n_{H_9} n_{V_{11}} \rangle$	$\langle n_{V_9} n_{V_{11}} \rangle$	$-\langle n_{V_{1'}} n_{H_{11}} \rangle$	$-\langle n_{V_{1'}} n_{V_{11}} \rangle$
	$\langle n_{H_{10}} n_{H_{11}} \rangle$	$\langle n_{V_{10}} n_{H_{11}} \rangle$	$\langle n_{H_{10}} n_{V_{11}} \rangle$	$\langle n_{V_{10}} n_{V_{11}} \rangle$	$-\langle n_{V_{1'}} n_{H_{11}} \rangle$	$-\langle n_{V_{1'}} n_{V_{11}} \rangle$
$H_{1in} H_{2in}$	1/8	0	0	0	0	0
$H_{1in} V_{2in}$	0	1/8	0	0	0	0
$V_{1in} H_{2in}$	0	0	1/8	0	0	0
$V_{1in} V_{2in}$	0	0	0	1/8	0	0
$V_{1'in} H_{2in}$	0	0	0	0	1/8	0
$V_{1'in} V_{2in}$	0	0	0	0	0	1/8

and 12), the P-SWAP gate is completed. When the outing components emitting from 9, 1', and 11 (or from 10, 1' and 11), the gate can also be completed by setting a feed-forward phase shifter  $P_\pi$  in mode 1' which achieves the transformations  $-\alpha_5|V\rangle_{1'}|H\rangle_{11} \xrightarrow{P_\pi} \alpha_5|V\rangle_{1'}|H\rangle_{11}$  and  $-\alpha_6|V\rangle_{1'}|V\rangle_{11} \xrightarrow{P_\pi} \alpha_6|V\rangle_{1'}|V\rangle_{11}$ . Based on the spatial modes of the outing photons, the classical feed-forward operations can work correctly. Therefore, the quantum circuit shown in Fig. 4 completes a linear optical P-SWAP gate in the coincidence basis with a success probability of 1/2. The success (or the output modes) of the scheme can be heralded by using the success instances in the post-selection in the applications.

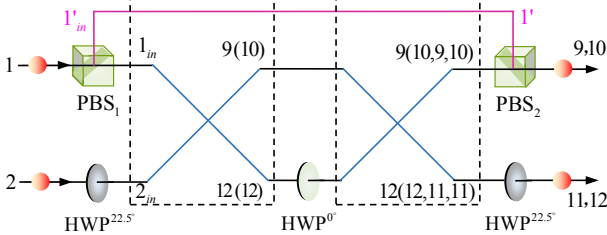


Figure 5: Implementation of a linear optical CNOT gate. The operation in the dotted rectangle is a P-SWAP gate, as shown in Fig. 4. The numbers represent input-output modes.

As shown in Fig. 5, a P-SWAP-based CNOT gate can be realized in the coincidence basis with linear optical elements. PBS plays a role in the qutrit  $X_A$  to provide an additional spatial mode. The operation in the black dotted rectangle corresponds to a P-SWAP gate in Fig. 4.

First, the initial state of the two injected photons is

tons is

$$|\chi_0\rangle = \alpha_1|H\rangle_1|H\rangle_2 + \alpha_2|H\rangle_1|V\rangle_2 + \alpha_3|V\rangle_1|H\rangle_2 + \alpha_4|V\rangle_1|V\rangle_2. \quad (21)$$

Second, photons 1 and 2 execute a PBS<sub>1</sub> and an HWP<sup>22.5°</sup>, respectively, to pass through the first P-SWAP gate. After the photons interact with the first P-SWAP gate, the outing photons emitted from modes 9, 1', and 12, and 10, 1', and 12 (without feed-forward operations) will be led to the next HWP<sup>0°</sup> and the rightmost P-SWAP gate, and then,  $|\chi_0\rangle$  is changed to  $|\chi_{i,12}\rangle$ ,  $i \in \{9, 10\}$ . Here,

$$|\chi_{i,12}\rangle = \frac{1}{\sqrt{2}}[\alpha_1(|H\rangle_i + |V\rangle_i)|H\rangle_{12} + \alpha_2(|H\rangle_i - |V\rangle_i)|H\rangle_{12} + \alpha_3|V\rangle_{1'}(|H\rangle_{12} + |V\rangle_{12}) + \alpha_4|V\rangle_{1'}(|H\rangle_{12} - |V\rangle_{12})]. \quad (22)$$

Third, HWP<sup>0°</sup> acts on mode 12 to complete  $|H\rangle_{12} \rightarrow |H\rangle_{12}$  and  $|V\rangle_{12} \rightarrow -|V\rangle_{12}$ . The second P-SWAP gate produces eight desired outcomes of the system, that is, (i) when the photons emitted from modes 9, 1', and 11, the state  $|\chi_{i,12}\rangle$  will collapse into

$$|\chi_{i,9,11}^-\rangle = \frac{1}{\sqrt{2}}[\alpha_1|H\rangle_9(|H\rangle_{11} + |V\rangle_{11}) + \alpha_2|H\rangle_9(|H\rangle_{11} - |V\rangle_{11}) - \alpha_3|V\rangle_{1'}(|H\rangle_{11} - |V\rangle_{11}) - \alpha_4|V\rangle_{1'}(|H\rangle_{11} + |V\rangle_{11})]. \quad (23)$$

(ii) When the photons emitted from modes 10, 1',

and 11, the state  $|\chi_{i,12}\rangle$  will collapse into

$$\begin{aligned} |\chi_{i,10,11}^-\rangle &= \frac{1}{\sqrt{2}}[\alpha_1|H\rangle_{10}(|H\rangle_{11} + |V\rangle_{11}) \\ &\quad + \alpha_2|H\rangle_{10}(|H\rangle_{11} - |V\rangle_{11}) \\ &\quad - \alpha_3|V\rangle_{1'}(|H\rangle_{11} - |V\rangle_{11}) \\ &\quad - \alpha_4|V\rangle_{1'}(|H\rangle_{11} + |V\rangle_{11})]. \end{aligned} \quad (24)$$

(iii) When the photons emitted from modes 9, 1', and 12, the state  $|\chi_{i,12}\rangle$  will collapse into

$$\begin{aligned} |\chi_{i,9,12}^+\rangle &= \frac{1}{\sqrt{2}}[\alpha_1|H\rangle_9(|H\rangle_{12} + |V\rangle_{12}) \\ &\quad + \alpha_2|H\rangle_9(|H\rangle_{12} - |V\rangle_{12}) \\ &\quad + \alpha_3|V\rangle_{1'}(|H\rangle_{12} - |V\rangle_{12}) \\ &\quad + \alpha_4|V\rangle_{1'}(|H\rangle_{12} + |V\rangle_{12})]. \end{aligned} \quad (25)$$

(iv) When the photons emitted from modes 10, 1', and 12, the state  $|\chi_{i,12}\rangle$  will collapse into

$$\begin{aligned} |\chi_{i,10,12}^+\rangle &= \frac{1}{\sqrt{2}}[\alpha_1|H\rangle_{10}(|H\rangle_{12} + |V\rangle_{12}) \\ &\quad + \alpha_2|H\rangle_{10}(|H\rangle_{12} - |V\rangle_{12}) \\ &\quad + \alpha_3|V\rangle_{1'}(|H\rangle_{12} - |V\rangle_{12}) \\ &\quad + \alpha_4|V\rangle_{1'}(|H\rangle_{12} + |V\rangle_{12})]. \end{aligned} \quad (26)$$

Finally, modes 9 (10) and 1' are combined into the same mode by PBS<sub>2</sub>, and HWP<sup>22.5°</sup> is applied to mode 12 (11) again. After PBS<sub>2</sub> and HWP<sup>22.5°</sup>, we obtain  $|\chi_{9,12}^+\rangle'$ ,  $|\chi_{10,12}^+\rangle'$ ,  $|\chi_{9,11}^-\rangle'$ , and  $|\chi_{10,11}^-\rangle'$ . That is,  $|\chi_{i,j}^\pm\rangle'$  with  $i \in \{9, 10\}$  and  $j \in \{11, 12\}$  is described by

$$\begin{aligned} |\chi_{i,j}^\pm\rangle' &= \alpha_1|H\rangle_i|H\rangle_j + \alpha_2|H\rangle_i|V\rangle_j \\ &\quad \pm \alpha_3|V\rangle_i|V\rangle_j \pm \alpha_4|V\rangle_i|H\rangle_j. \end{aligned} \quad (27)$$

The minus signs of  $|\chi_{9,11}^-\rangle'$  and  $|\chi_{10,11}^-\rangle'$  can be corrected by setting the HWP<sup>0°</sup> to modes 9 and 10 when two outgoing photons are at output ports 9 and 11, or 10 and 11. That is, after the feed-forward operations are only applied to the rightmost P-SWAP gate, an optical post-selection CNOT gate with a success probability of  $1/8 = 1/4 \times 1/2$  is completed. Remarkably, additional entangled photon pairs or single photons are necessary for previous schemes [52–55], but are not required for our CNOT gate. In addition, the success probability of the gate is improved on the results without an auxiliary photon [56–58].

As shown in Fig. 6, after three input photons are injected into modes 1, 2, and 3, the initial

state is given by

$$\begin{aligned} |\Xi_0\rangle &= \alpha_1|H\rangle_1|H\rangle_2|H\rangle_3 \\ &\quad + \alpha_2|H\rangle_1|H\rangle_2|V\rangle_3 \\ &\quad + \alpha_3|H\rangle_1|V\rangle_2|H\rangle_3 \\ &\quad + \alpha_4|H\rangle_1|V\rangle_2|V\rangle_3 \\ &\quad + \alpha_5|V\rangle_1|H\rangle_2|H\rangle_3 \\ &\quad + \alpha_6|V\rangle_1|H\rangle_2|V\rangle_3 \\ &\quad + \alpha_7|V\rangle_1|V\rangle_2|H\rangle_3 \\ &\quad + \alpha_8|V\rangle_1|V\rangle_2|V\rangle_3. \end{aligned} \quad (28)$$

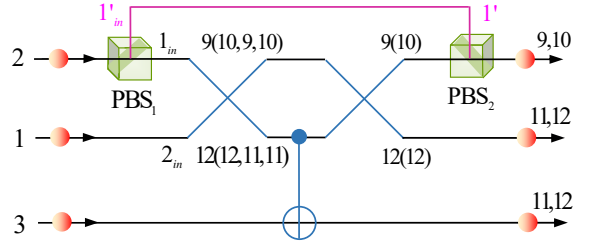


Figure 6: Optical implementation of a three-photon Toffoli gate.

First, after photons go through the PBS<sub>1</sub> and the leftmost P-SWAP gate, when we choose the output modes 9, 1' and 12, and 10, 1' and 12 (9, 1' and 11, and 10, 1' and 11 with the classical feed-forward operations), we can obtain four desired outcomes,

$$\begin{aligned} |\Xi_{1a}\rangle &= \frac{1}{2\sqrt{2}}[\alpha_1|H\rangle_{12}|H\rangle_9|H\rangle_3 \\ &\quad + \alpha_2|H\rangle_{12}|H\rangle_9|V\rangle_3 \\ &\quad + \alpha_3|H\rangle_{12}|V\rangle_{1'}|H\rangle_3 \\ &\quad + \alpha_4|H\rangle_{12}|V\rangle_{1'}|V\rangle_3 \\ &\quad + \alpha_5|H\rangle_{12}|V\rangle_9|H\rangle_3 \\ &\quad + \alpha_6|H\rangle_{12}|V\rangle_9|V\rangle_3 \\ &\quad + \alpha_7|V\rangle_{12}|V\rangle_{1'}|H\rangle_3 \\ &\quad + \alpha_8|V\rangle_{12}|V\rangle_{1'}|V\rangle_3], \end{aligned} \quad (29)$$

$$\begin{aligned} |\Xi_{1b}\rangle &= \frac{1}{2\sqrt{2}}[\alpha_1|H\rangle_{12}|H\rangle_{10}|H\rangle_3 \\ &\quad + \alpha_2|H\rangle_{12}|H\rangle_{10}|V\rangle_3 \\ &\quad + \alpha_3|H\rangle_{12}|V\rangle_{1'}|H\rangle_3 \\ &\quad + \alpha_4|H\rangle_{12}|V\rangle_{1'}|V\rangle_3 \\ &\quad + \alpha_5|H\rangle_{12}|V\rangle_{10}|H\rangle_3 \\ &\quad + \alpha_6|H\rangle_{12}|V\rangle_{10}|V\rangle_3 \\ &\quad + \alpha_7|V\rangle_{12}|V\rangle_{1'}|H\rangle_3 \\ &\quad + \alpha_8|V\rangle_{12}|V\rangle_{1'}|V\rangle_3], \end{aligned} \quad (30)$$

$$\begin{aligned}
|\Xi_{1c}\rangle = & \frac{1}{2\sqrt{2}}[\alpha_1|H\rangle_{11}|H\rangle_9|H\rangle_3 \\
& + \alpha_2|H\rangle_{11}|H\rangle_9|V\rangle_3 \\
& + \alpha_3|H\rangle_{11}|V\rangle_{1'}|H\rangle_3 \\
& + \alpha_4|H\rangle_{11}|V\rangle_{1'}|V\rangle_3 \\
& + \alpha_5|H\rangle_{11}|V\rangle_9|H\rangle_3 \\
& + \alpha_6|H\rangle_{11}|V\rangle_9|V\rangle_3 \\
& + \alpha_7|V\rangle_{11}|V\rangle_{1'}|H\rangle_3 \\
& + \alpha_8|V\rangle_{11}|V\rangle_{1'}|V\rangle_3],
\end{aligned} \tag{31}$$

$$\begin{aligned}
|\Xi_{1d}\rangle = & \frac{1}{2\sqrt{2}}[\alpha_1|H\rangle_{11}|H\rangle_{10}|H\rangle_3 \\
& + \alpha_2|H\rangle_{11}|H\rangle_{10}|V\rangle_3 \\
& + \alpha_3|H\rangle_{11}|V\rangle_{1'}|H\rangle_3 \\
& + \alpha_4|H\rangle_{11}|V\rangle_{1'}|V\rangle_3 \\
& + \alpha_5|H\rangle_{11}|V\rangle_{10}|H\rangle_3 \\
& + \alpha_6|H\rangle_{11}|V\rangle_{10}|V\rangle_3 \\
& + \alpha_7|V\rangle_{11}|V\rangle_{1'}|H\rangle_3 \\
& + \alpha_8|V\rangle_{11}|V\rangle_{1'}|V\rangle_3].
\end{aligned} \tag{32}$$

Second, the CNOT gate acts on photon 1 and photon 3, which can yield 16 desired outcomes  $|\Xi_{i,j,k}\rangle$  (two-fold). Here,  $|\Xi_{i,j,k}\rangle$  with  $i \in \{9, 10\}$ ,  $j \in \{9, 10\}$  and  $k \in \{11, 12\}$ , is described by

$$\begin{aligned}
|\Xi_{i,j,k}\rangle = & \frac{1}{2\sqrt{2}}[\alpha_1|H\rangle_i|H\rangle_j|H\rangle_k \\
& + \alpha_2|H\rangle_i|H\rangle_j|V\rangle_k \\
& + \alpha_3|H\rangle_i|V\rangle_{1'}|H\rangle_k \\
& + \alpha_4|H\rangle_i|V\rangle_{1'}|V\rangle_k \\
& + \alpha_5|H\rangle_i|V\rangle_j|H\rangle_k \\
& + \alpha_6|H\rangle_i|V\rangle_j|V\rangle_k \\
& + \alpha_7|V\rangle_i|V\rangle_{1'}|V\rangle_k \\
& + \alpha_8|V\rangle_i|V\rangle_{1'}|H\rangle_k].
\end{aligned} \tag{33}$$

Third, after the rightmost P-SWAP gate acts on photon 1 and photon 2, when we choose the output modes 9, 1' and 12 (10, 1' and 12), we can obtain 32 desired outcomes  $|\Xi_{12,j,k}\rangle$  (eight-fold). Here,  $|\Xi_{12,j,k}\rangle$  with  $j \in \{9, 10\}$  and  $k \in \{11, 12\}$ ,

is described by

$$\begin{aligned}
|\Xi_{12,j,k}\rangle = & \frac{1}{8}[\alpha_1|H\rangle_{12}|H\rangle_j|H\rangle_k \\
& + \alpha_2|H\rangle_{12}|H\rangle_j|V\rangle_k \\
& + \alpha_3|H\rangle_{12}|V\rangle_{1'}|H\rangle_k \\
& + \alpha_4|H\rangle_{12}|V\rangle_{1'}|V\rangle_k \\
& + \alpha_5|V\rangle_{12}|H\rangle_j|H\rangle_k \\
& + \alpha_6|V\rangle_{12}|H\rangle_j|V\rangle_k \\
& + \alpha_7|V\rangle_{12}|V\rangle_{1'}|V\rangle_k \\
& + \alpha_8|V\rangle_{12}|V\rangle_{1'}|H\rangle_k].
\end{aligned} \tag{34}$$

Finally, photons in modes 9 (10) and 1' can be combined into the same mode by a PBS<sub>2</sub>. Therefore, the linear optical Toffoli gate can be achieved without auxiliary photons. Our proposal has a higher success probability ( $1/64 = 1/2 \times 1/8 \times 1/4$ ) than the simplified CNOT-based one ( $1/72$ ) [19, 20] and the one without a decomposition-based approach ( $1/133$ ) [51]. In addition, optical single-qudit operation ensembles  $X_a, X_b, \dots, X_n$  can be achieved by employing a sequence of PBSs, and the linear optical  $n$ -control-photon Toffoli gate can be implemented in principle (see Fig. 7).

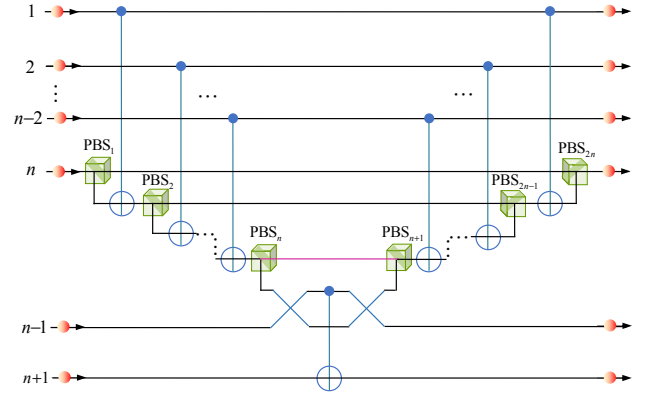


Figure 7: Implementation of an  $(n+1)$ -photon Toffoli gate.

## 4 Discussion and Conclusion

The optimal cost of a Toffoli gate is six CNOT gates using the standard decomposition-based approach [39]. The theoretical lower bound of a Toffoli gate is five two-qubit gates [40]. Ralph *et al.* [19] first reduced the cost of a Toffoli gate to three CNOT gates by introducing auxiliary Hilbert space. Inspired by traditional all

CNOT gate synthesis [19, 20], the quantum circuit we designed to implement the Toffoli gate possesses the higher success probability than the protocols in Refs. [19, 20] with the same cost in terms of required qubit-qudit gates. The required qubit-qudit entangled gates are all nearest neighbors in our construction of the three-qubit Toffoli gate. Note that the nearest-neighbor quantum gate where each qubit interacts only with its nearest neighbors requires less resource overhead than the long-range one. For example, a long-range CNOT gate acting on the first qubit and the third qubit is constructed by four nearest-neighbor CNOT gates [59]. In addition,  $(2n - 3)$  qubit-qudit gates can simulate an  $n$ -qubit Toffoli gate in higher-dimensional spaces, which considerably improves on the previous result with  $O(n^2)$  [1].

Linear optics has inherent probability characteristics for the implementation of controlled quantum gates. With the help of an additional entangled photon pair [53, 54] or a single photon [55], optical CNOT gate with a success probability of  $1/4$  or  $1/8$  can be realistically implemented. Without auxiliary photons, CNOT gate with a success probability of  $1/9$  has been experimentally demonstrated in linear optics [56–58]. Remarkably, the success probability of our P-SWAP-based CNOT gate is enhanced to  $1/8$  without additional photons. Moreover, the success probability of our P-SWAP-based Toffoli gate ( $1/64$ ) is higher than the CNOT-based protocols ( $1/72$ ) [19, 20] and it is also higher than the no-decomposition-based one ( $1/133$ ) [51].

The multi-level system is essential to realize our schemes. In optical system, we can encode polarization DOF of photons as two computational qubits and spatial-mode DOF as the qudit (extra level). We can also encode these levels on orbital angular momentum of photons. Besides, diamond nitrogen-vacancy defect center [60, 61] and superconducting system [62, 63] can also provide available multiple levels to implement the universal quantum gates due to their long coherence time and flexible manipulation.

In summary, by introducing higher-dimensional spaces, we proposed simplified CNOT and Toffoli gates. A three-qubit Toffoli gate can be simulated with two P-SWAP, one CNOT, and two single-qudit gates.  $(2n - 3)$  qubit-qudit gates and  $(2n - 4)$  single-qudit gates

are sufficient for constructing an  $n$ -qubit Toffoli gate. Following the simplified synthesis, as a feasible example, linear optics architectures for implementing CNOT and Toffoli gates were designed with a higher success probability.

## Acknowledgments

This work is supported by the National Natural Science Foundation of China under Grant No. 11604012, the Fundamental Research Funds for the Central Universities under Grants No. FRF-BR-19-011A3 and No. 230201506500024, and a grant from the China Scholarship Council. L.-C.K. is supported by the Ministry of Education and the National Research Foundation Singapore.

## References

- [1] Adriano Barenco, Charles H Bennett, Richard Cleve, David P DiVincenzo, Norman Margolus, Peter Shor, Tycho Sleator, John A Smolin, and Harald Weinfurter. Elementary gates for quantum computation. *Physical Review A*, 52(5):3457, 1995. DOI: [10.1103/PhysRevA.52.3457](https://doi.org/10.1103/PhysRevA.52.3457).
- [2] Lov K Grover. Quantum mechanics helps in searching for a needle in a haystack. *Physical Review Letters*, 79(2):325, 1997. DOI: [10.1103/PhysRevLett.79.325](https://doi.org/10.1103/PhysRevLett.79.325).
- [3] Peter W Shor. Polynomial-time algorithms for prime factorization and discrete logarithms on a quantum computer. *SIAM Review*, 41(2):303–332, 1999. DOI: [10.1137/S0036144598347011](https://doi.org/10.1137/S0036144598347011).
- [4] Caroline Figgatt, Dmitri Maslov, KA Landsman, Norbert Matthias Linke, Shantanu Debnath, and C Monroe. Complete 3-qubit Grover search on a programmable quantum computer. *Nature Communications*, 8(1):1918, 2017. DOI: [10.1038/s41467-017-01904-7](https://doi.org/10.1038/s41467-017-01904-7).
- [5] Yunseong Nam, Yuan Su, and Dmitri Maslov. Approximate quantum Fourier transform with  $o(n \log(n))$  T gates. *npj Quantum Information*, 6(1):26, 2020. DOI: [10.1038/s41534-020-0257-5](https://doi.org/10.1038/s41534-020-0257-5).
- [6] Nicolas Gisin, Grégoire Ribordy, Wolfgang Tittel, and Hugo Zbinden. Quantum cryptography. *Reviews of Modern Physics*,

- 74(1):145, 2002. DOI: [10.1103/RevModPhys.74.145](https://doi.org/10.1103/RevModPhys.74.145).
- [7] Michael A Nielsen and Isaac L Chuang. *Quantum Computation and Quantum Information: 10th Anniversary Edition*. Cambridge University Press, 2010. DOI: [10.1017/CBO9780511976667](https://doi.org/10.1017/CBO9780511976667).
- [8] Vivek V Shende, Igor L Markov, and Stephen S Bullock. Minimal universal two-qubit controlled-NOT-based circuits. *Physical Review A*, 69(6):062321, 2004. DOI: [10.1103/PhysRevA.69.062321](https://doi.org/10.1103/PhysRevA.69.062321).
- [9] Navin Khaneja and Steffen J Glaser. Cartan decomposition of  $SU(2^n)$  and control of spin systems. *Chemical Physics*, 267(1-3):11–23, 2001. DOI: [10.1016/S0301-0104\(01\)00318-4](https://doi.org/10.1016/S0301-0104(01)00318-4).
- [10] Mikko Möttönen, Juha J Vartiainen, Ville Bergholm, and Martti M Salomaa. Quantum circuits for general multiqubit gates. *Physical Review Letters*, 93(13):130502, 2004. DOI: [10.1103/PhysRevLett.93.130502](https://doi.org/10.1103/PhysRevLett.93.130502).
- [11] Stephen S Bullock and Gavin K Brennen. Canonical decompositions of  $n$ -qubit quantum computations and concurrence. *Journal of Mathematical Physics*, 45(6):2447–2467, 2004. DOI: [10.1063/1.17237012](https://doi.org/10.1063/1.17237012).
- [12] Vivek V Shende, Stephen S Bullock, and Igor L Markov. Synthesis of quantum-logic circuits. *IEEE Transactions on Computer-Aided Design of Integrated Circuits and Systems*, 25(6):1000–1010, 2006. DOI: [10.1109/TCAD.2005.855930](https://doi.org/10.1109/TCAD.2005.855930).
- [13] Domenico D’Alessandro and Francesca Albertini. Quantum symmetries and Cartan decompositions in arbitrary dimensions. *Journal of Physics A: Mathematical and Theoretical*, 40(10):2439, 2007. DOI: [10.1088/1751-8113/40/10/013](https://doi.org/10.1088/1751-8113/40/10/013).
- [14] Yao Min Di and Hai Rui Wei. Synthesis of multivalued quantum logic circuits by elementary gates. *Physical Review A*, 87(1):012325, 2013. DOI: [10.1103/PhysRevA.87.012325](https://doi.org/10.1103/PhysRevA.87.012325).
- [15] Raban Iten, Roger Colbeck, Ivan Kukuljan, Jonathan Home, and Matthias Christandl. Quantum circuits for isometries. *Physical Review A*, 93(3):032318, 2016. DOI: [10.1103/PhysRevA.93.032318](https://doi.org/10.1103/PhysRevA.93.032318).
- [16] Farrokh Vatan and Colin Williams. Optimal quantum circuits for general two-qubit gates. *Physical Review A*, 69(3):032315, 2004. DOI: [10.1103/PhysRevA.69.032315](https://doi.org/10.1103/PhysRevA.69.032315).
- [17] Guifre Vidal and Christopher M Dawson. Universal quantum circuit for two-qubit transformations with three controlled-NOT gates. *Physical Review A*, 69(1):010301(R), 2004. DOI: [10.1103/PhysRevA.69.010301](https://doi.org/10.1103/PhysRevA.69.010301).
- [18] Vivek V Shende, Stephen S Bullock, and Igor L Markov. Recognizing small-circuit structure in two-qubit operators. *Physical Review A*, 70(1):012310, 2004. DOI: [10.1103/PhysRevA.70.012310](https://doi.org/10.1103/PhysRevA.70.012310).
- [19] T C Ralph, K J Resch, and Alexei Gilchrist. Efficient Toffoli gates using qudits. *Physical Review A*, 75(2):022313, 2007. DOI: [10.1103/PhysRevA.75.022313](https://doi.org/10.1103/PhysRevA.75.022313).
- [20] Benjamin P Lanyon, Marco Barbieri, Marcelo P Almeida, Thomas Jennewein, Timothy C Ralph, Kevin J Resch, Geoff J Pryde, Jeremy L O’Brien, Alexei Gilchrist, and Andrew G White. Simplifying quantum logic using higher-dimensional Hilbert spaces. *Nature Physics*, 5(2):134–140, 2009. DOI: [10.1038/nphys1150](https://doi.org/10.1038/nphys1150).
- [21] Arkady Fedorov, Lars Steffen, Matthias Baur, Marcus P da Silva, and Andreas Wallraff. Implementation of a Toffoli gate with superconducting circuits. *Nature*, 481(7380):170–172, 2012. DOI: [10.1038/nature10713](https://doi.org/10.1038/nature10713).
- [22] Kai Liu, Wen Dong Li, Wen Zhao Zhang, Peng Shi, Chun Nian Ren, and Yong Jian Gu. Optimizing quantum circuits using higher-dimensional Hilbert spaces. *Acta Physica Sinica*, 61(12):120301, 2012. DOI: [10.7498/aps.61.120301](https://doi.org/10.7498/aps.61.120301).
- [23] Wen Dong Li, Yong Jian Gu, Kai Liu, Yuan Harnng Lee, and Yao Zhong Zhang. Efficient universal quantum computation with auxiliary Hilbert space. *Physical Review A*, 88(3):034303, 2013. DOI: [10.1103/PhysRevA.88.034303](https://doi.org/10.1103/PhysRevA.88.034303).
- [24] Wen Qiang Liu and Hai Rui Wei. Optimal synthesis of the Fredkin gate in a multilevel system. *New Journal of Physics*, 22(6):063026, 2020. DOI: [10.1088/1367-2630/ab8e13](https://doi.org/10.1088/1367-2630/ab8e13).
- [25] Wen Qiang Liu, Hai Rui Wei, and Leong Chuan Kwek. Low-cost Fredkin gate with auxiliary space. *Physical Review Applied*, 14(5):054057, 2020. DOI: [10.1103/PhysRevApplied.14.054057](https://doi.org/10.1103/PhysRevApplied.14.054057).

- [26] Nicolas J Cerf, Mohamed Bourennane, Anders Karlsson, and Nicolas Gisin. Security of quantum key distribution using  $d$ -level systems. *Physical Review Letters*, 88(12):127902, 2002. DOI: [10.1103/PhysRevLett.88.127902](https://doi.org/10.1103/PhysRevLett.88.127902).
- [27] Mehul Malik, Manuel Erhard, Marcus Huber, Mario Krenn, Robert Fickler, and Anton Zeilinger. Multi-photon entanglement in high dimensions. *Nature Photonics*, 10(4):248–252, 2016. DOI: [10.1038/nphoton.2016.12](https://doi.org/10.1038/nphoton.2016.12).
- [28] Yingwen Zhang, Megan Agnew, Thomas Roger, Filippus S Roux, Thomas Konrad, Daniele Faccio, Jonathan Leach, and Andrew Forbes. Simultaneous entanglement swapping of multiple orbital angular momentum states of light. *Nature Communications*, 8(1):632, 2017. DOI: [10.1038/s41467-017-00706-1](https://doi.org/10.1038/s41467-017-00706-1).
- [29] Feiran Wang, Manuel Erhard, Amin Babazadeh, Mehul Malik, Mario Krenn, and Anton Zeilinger. Generation of the complete four-dimensional Bell basis. *Optica*, 4(12):1462–1467, 2017. DOI: [10.1364/OP-TICA.4.001462](https://doi.org/10.1364/OP-TICA.4.001462).
- [30] Xiao Min Hu, Yu Guo, Bi Heng Liu, Yun Feng Huang, Chuan Feng Li, and Guang Can Guo. Beating the channel capacity limit for superdense coding with entangled ququarts. *Science Advances*, 4(7):eaat9304, 2018. DOI: [10.1126/sciadv.aat9304](https://doi.org/10.1126/sciadv.aat9304).
- [31] Yi Han Luo, Han Sen Zhong, Manuel Erhard, Xi Lin Wang, Li Chao Peng, Mario Krenn, Xiao Jiang, Li Li, Nai Le Liu, Chao Yang Lu, A Zeilinger, and J W Pan. Quantum teleportation in high dimensions. *Physical Review Letters*, 123(7):070505, 2019. DOI: [10.1103/PhysRevLett.123.070505](https://doi.org/10.1103/PhysRevLett.123.070505).
- [32] Xiao Min Hu, Chao Zhang, Bi Heng Liu, Yu Cai, Xiang Jun Ye, Yu Guo, Wen Bo Xing, Cen Xiao Huang, Yun Feng Huang, Chuan Feng Li, and Guang Can Guo. Experimental high-dimensional quantum teleportation. *Physical Review Letters*, 125(23):230501, 2020. DOI: [10.1103/PhysRevLett.125.230501](https://doi.org/10.1103/PhysRevLett.125.230501).
- [33] Vincenzo D’ambrosio, Nicolò Spagnolo, Lorenzo Del Re, Sergei Slussarenko, Ying Li, Leong Chuan Kwek, Lorenzo Marrucci, Stephen P Walborn, Leandro Aolita, and Fabio Sciarrino. Photonic polarization gears for ultra-sensitive angular measurements. *Nature Communications*, 4(9):2432, 2013. DOI: [10.1038/ncomms3432](https://doi.org/10.1038/ncomms3432).
- [34] Yaoyun Shi. Both Toffoli and controlled-NOT need little help to do universal quantum computation. *Quantum Information and Computation*, 3(1):84–92, 2002. DOI: [10.1016/S0146-6410\(03\)00082-6](https://doi.org/10.1016/S0146-6410(03)00082-6).
- [35] David G Cory, MD Price, W Maas, Emanuel Knill, Raymond Laflamme, Wojciech H Zurek, Timothy F Havel, and Shyamal S Somaroo. Experimental quantum error correction. *Physical Review Letters*, 81(10):2152, 1998. DOI: [10.1103/PhysRevLett.81.2152](https://doi.org/10.1103/PhysRevLett.81.2152).
- [36] Matthew D Reed, Leonardo DiCarlo, Simon E Nigg, Luyan Sun, Luigi Frunzio, Steven M Girvin, and Robert J Schoelkopf. Realization of three-qubit quantum error correction with superconducting circuits. *Nature*, 482(7385):382–385, 2012. DOI: [10.1038/nature10786](https://doi.org/10.1038/nature10786).
- [37] Adam Paetznick and Ben W Reichardt. Universal fault-tolerant quantum computation with only transversal gates and error correction. *Physical Review Letters*, 111(9):090505, 2013. DOI: [10.1103/PhysRevLett.111.090505](https://doi.org/10.1103/PhysRevLett.111.090505).
- [38] Jérémie Guillaud and Mazyar Mirrahimi. Repetition cat qubits for fault-tolerant quantum computation. *Physical Review X*, 9(4):041053, 2019. DOI: [10.1103/PhysRevX.9.041053](https://doi.org/10.1103/PhysRevX.9.041053).
- [39] Vivek V Shende and Igor L Markov. On the CNOT-cost of Toffoli gates. *Quantum Information and Computation*, 9(5):461–486, 2008. DOI: [10.1134/S1063779609030058](https://doi.org/10.1134/S1063779609030058).
- [40] Nengkun Yu, Runyao Duan, and Mingsheng Ying. Five two-qubit gates are necessary for implementing the Toffoli gate. *Physical Review A*, 88(1):010304(R), 2013. DOI: [10.1103/PhysRevA.88.010304](https://doi.org/10.1103/PhysRevA.88.010304).
- [41] Nengkun Yu and Mingsheng Ying. Optimal simulation of Deutsch gates and the Fredkin gate. *Physical Review A*, 91(3):032302, 2015. DOI: [10.1103/PhysRevA.91.032302](https://doi.org/10.1103/PhysRevA.91.032302).
- [42] E O Kiktenko, A S Nikolaeva, Peng Xu, G V Shlyapnikov, and A K Fedorov. Scalable quantum computing with qudits on a

- graph. *Physical Review A*, 101(2):022304, 2020. DOI: [10.1103/PhysRevA.101.022304](https://doi.org/10.1103/PhysRevA.101.022304).
- [43] M Mičuda, Michal Sedlak, Ivo Straka, Martina Miková, M Dušek, M Ježek, and J Fiurášek. Efficient experimental estimation of fidelity of linear optical quantum Toffoli gate. *Physical Review Letters*, 111(16):160407, 2013. DOI: [10.1103/PhysRevLett.111.160407](https://doi.org/10.1103/PhysRevLett.111.160407).
- [44] Karel Lemr, Karol Bartkiewicz, Antonín Černoš, Miloslav Dušek, and Jan Soubusta. Experimental implementation of optimal linear-optical controlled-unitary gates. *Physical Review Letters*, 114(15):153602, 2015. DOI: [10.1103/PhysRevLett.114.153602](https://doi.org/10.1103/PhysRevLett.114.153602).
- [45] M Mičuda, M Miková, I Straka, M Sedlák, M Dušek, M Ježek, and J Fiurášek. Tomographic characterization of a linear optical quantum Toffoli gate. *Physical Review A*, 92(3):032312, 2015. DOI: [10.1103/PhysRevA.92.032312](https://doi.org/10.1103/PhysRevA.92.032312).
- [46] Shihao Ru, Yunlong Wang, Min An, Feiran Wang, Pei Zhang, and Fuli Li. Realization of deterministic quantum Toffoli gate with a single photon. *Physical Review A*, 103(2):022606, 2021. DOI: [10.1103/PhysRevA.103.022606](https://doi.org/10.1103/PhysRevA.103.022606).
- [47] Thomas Monz, Kihwan Kim, Wolfgang Hänsel, M Riebe, AS Villar, Philipp Schindler, Michael Chwalla, Markus Hennrich, and Rainer Blatt. Realization of the quantum Toffoli gate with trapped ions. *Physical Review Letters*, 102(4):040501, 2009. DOI: [10.1103/PhysRevLett.102.040501](https://doi.org/10.1103/PhysRevLett.102.040501).
- [48] I I Beterov, I N Ashkarin, E A Yakshina, D B Tretyakov, V M Entin, I I Ryabtsev, P Cheinet, P Pillet, and M Saffman. Fast three-qubit Toffoli quantum gate based on three-body Förster resonances in Rydberg atoms. *Physical Review A*, 98(4):042704, 2018. DOI: [10.1103/PhysRevA.98.042704](https://doi.org/10.1103/PhysRevA.98.042704).
- [49] Harry Levine, Alexander Keesling, Giulia Semeghini, Ahmed Omran, Tout T Wang, Sepehr Ebadi, Hannes Bernien, Markus Greiner, Vladan Vuletić, Hannes Pichler, and M D Lukin. Parallel implementation of high-fidelity multiqubit gates with neutral atoms. *Physical Review Letters*, 123(17):170503, 2019. DOI: [10.1103/PhysRevLett.123.170503](https://doi.org/10.1103/PhysRevLett.123.170503).
- [50] M J Gullans and J R Petta. Protocol for a resonantly driven three-qubit Toffoli gate with silicon spin qubits. *Physical Review B*, 100(8):085419, 2019. DOI: [10.1103/PhysRevB.100.085419](https://doi.org/10.1103/PhysRevB.100.085419).
- [51] Jaromír Fiurášek. Linear-optics quantum Toffoli and Fredkin gates. *Physical Review A*, 73(6):062313, 2006. DOI: [10.1103/PhysRevA.73.062313](https://doi.org/10.1103/PhysRevA.73.062313).
- [52] T B Pittman, B C Jacobs, and J D Franson. Probabilistic quantum logic operations using polarizing beam splitters. *Physical Review A*, 64(6):062311, 2001. DOI: [10.1103/PhysRevA.64.062311](https://doi.org/10.1103/PhysRevA.64.062311).
- [53] Sara Gasparoni, Jian Wei Pan, Philip Walther, Terry Rudolph, and Anton Zeilinger. Realization of a photonic CNOT gate sufficient for quantum computation. *Physical Review Letters*, 93(2):020504, 2004. DOI: [10.1103/PhysRevLett.93.020504](https://doi.org/10.1103/PhysRevLett.93.020504).
- [54] Xiao Hui Bao, Teng Yun Chen, Qiang Zhang, Jian Yang, Han Zhang, Tao Yang, and Jian Wei Pan. Optical nondestructive controlled-NOT gate without using entangled photons. *Physical Review Letters*, 98(17):170502, 2007. DOI: [10.1103/PhysRevLett.98.170502](https://doi.org/10.1103/PhysRevLett.98.170502).
- [55] Jonas Zeuner, Aditya N Sharma, Max Tillmann, René Heilmann, Markus Gräfe, Amir Moqanaki, Alexander Szameit, and Philip Walther. Integrated-optics heralded controlled-NOT gate for polarization-encoded qubits. *npj Quantum Information*, 4(1):13, 2018. DOI: [10.1038/s41534-018-0068-0](https://doi.org/10.1038/s41534-018-0068-0).
- [56] Nathan K Langford, T J Weinhold, R Prevedel, K J Resch, Alexei Gilchrist, J L O'Brien, G J Pryde, and A G White. Demonstration of a simple entangling optical gate and its use in Bell-state analysis. *Physical Review Letters*, 95(21):210504, 2005. DOI: [10.1103/PhysRevLett.95.210504](https://doi.org/10.1103/PhysRevLett.95.210504).
- [57] Nikolai Kiesel, Christian Schmid, Ulrich Weber, Rupert Ursin, and Harald Weinfurter. Linear optics controlled-phase gate made simple. *Physical Review Letters*, 95(21):210505, 2005. DOI: [10.1103/PhysRevLett.95.210505](https://doi.org/10.1103/PhysRevLett.95.210505).
- [58] Ryo Okamoto, Holger F. Hofmann, Shigeki Takeuchi, and Keiji Sasaki. Demonstration of an optical quantum controlled-NOT

- gate without path interference. *Physical Review Letters*, 95(21):210506, 2005. DOI: [10.1103/PhysRevLett.95.210506](https://doi.org/10.1103/PhysRevLett.95.210506).
- [59] George F Viamontes, Igor L Markov, and John P Hayes. *Quantum circuit simulation*. Springer Science, 2009.
- [60] Ze Liang Xiang, Sahel Ashhab, J Q You, and Franco Nori. Hybrid quantum circuits: Superconducting circuits interacting with other quantum systems. *Reviews of Modern Physics*, 85(2):623, 2013. DOI: [10.1103/RevModPhys.85.623](https://doi.org/10.1103/RevModPhys.85.623).
- [61] Gerald Waldherr, Y Wang, S Zaiser, M Jamali, T Schulte-Herbrüggen, H Abe, T Ohshima, J Isoya, J F Du, P Neumann, and J Wrachtrup. Quantum error correction in a solid-state hybrid spin register. *Nature*, 506(7487):204–207, 2014. DOI: [10.1038/nature12919](https://doi.org/10.1038/nature12919).
- [62] Michael J Peterer, Samuel J Bader, Xiaoyue Jin, Fei Yan, Archana Kamal, Theodore J Gudmundsen, Peter J Leek, Terry P Orlando, William D Oliver, and Simon Gustavsson. Coherence and decay of higher energy levels of a superconducting transmon qubit. *Physical Review Letters*, 114(1):010501, 2015. DOI: [10.1103/PhysRevLett.114.010501](https://doi.org/10.1103/PhysRevLett.114.010501).
- [63] Thomas Bækkegaard, L B Kristensen, Niels J S Loft, Christian Kraglund Andersen, David Petrosyan, and Nikolaj T Zinner. Realization of efficient quantum gates with a superconducting qubit-qutrit circuit. *Scientific Reports*, 9(1):13389, 2019. DOI: [10.1038/s41598-019-49657-1](https://doi.org/10.1038/s41598-019-49657-1).